Pergamon

Int. J. Heat Mass Transfer. Vol. 41, No. 12, pp. 1845–1855, 1998
© 1998 Published by Elsevier Science Ltd. All rights reserved
Printed in Great Britain
0017–9310/98 $19.00+0.00

PII: S0017-9310(97)00254-8

Prediction of heat transfer in an axisymmetric turbulent jet impinging on a flat plate

M. BEHNIA† and S. PARNEIX
Center for Turbulence Research, Stanford University, Stanford, CA 94305-3030, U.S.A.

and

P. A. DURBIN
Mechanical Engineering Department, Stanford University, Stanford, CA 94305-3030, U.S.A.

(*Received* 23 *May* 1997)

Abstract—The problem of cooling of a heated plate by an axisymmetric isothermal fully developed turbulent jet has been studied numerically. Computations were performed with the normal-velocity relaxation turbulence model (V2F model). Local heat transfer coefficient predictions are compared to the available experimental data. For comparison, computations have also been carried out with the widely used k–ε model. The V2F heat transfer predictions are in excellent agreement with the experiments, whereas the k–ε model does not properly resolve the flow features, greatly over-predicts the rate of heat transfer and yields physically unrealistic behaviors. © 1998 Published by Elsevier Science Ltd. All rights reserved.

1. INTRODUCTION

Jet impingement heating and cooling is used in many engineering and industrial applications, such as materials processing, manufacturing, drying, and cooling of computers and electronic equipment. In most applications, a turbulent jet of gas or liquid is directed to the target area. A number of comprehensive reviews of jet impingement are available in the literature [1–3]. The advantages of impingement heat transfer process are direct, localized heating or cooling, and increased heat fluxes. This technique is an attractive, cost-effective method of cooling computers [4], especially in combination with heat sinks. A number of parameters must be considered in the design of such systems. For this reason, numerical prediction of the local heat transfer coefficient can expedite the design process. To this end, the flow and thermal fields must be accurately and economically computed; hence the need for better turbulence models.

Impinging jet flows have several features which make them a good vehicle for evaluation of turbulence models. In the impingement region, the mean flow is perpendicular (or nearly perpendicular) to the surface. It then turns and follows the surface in a wall jet (see Fig. 1). In the stagnation region, the flow is nearly irrotational and there is a large total strain along the stagnation streamline. Away from the core of the jet there is substantial curvature of the streamlines. Adjacent to the wall, there are thin stagnation points and wall jet boundary layers on the target plate.

The problem of a normal impinging jet of air striking a flat plate has been considered as a test case by ERCOFTAC; they adopted the flow measurements of Cooper *et al.* [5] and the heat transfer data of Baughn and Shimizu [6]. There are also a number of more recent heat transfer measurements by Baughn *et al.* [7], Yan [8], and Lytle and Webb [9]. These experimental data have been used by researchers to test turbulence models for this demanding case: for instance, Craft *et al.* [10] used the data of Cooper *et al.* [5] and Baughn and Shimizu [6] to examine the k–ε and three second-moment closure models in an axisymmetric geometry. Kunugi *et al.* [11] carried out a numerical and experimental study of a confined impinging jet and successfully used an anisotropic k–ε model.

The present paper reports computations of the flow and thermal fields in an axisymmetric isothermal fully developed turbulent jet, perpendicular to a uniform heat flux flat plate. The V2F model [12] was used in the calculations. The axisymmetric, incompressible, Reynolds averaged Navier-Stokes equations were solved in conjunction with the k–ε and v^2 transport equations, and the f elliptic relaxation equation (hence the acronym V2F model) on a finite-difference grid. Several turbulent Prandtl number formulas were examined. The computations are compared with a wide set of experimental data [5–9, 13]. For comparison, computations were also performed with the widely used standard k–ε model. The local heat trans-

† Author to whom correspondence should be addressed.

NOMENCLATURE

C_p	specific heat	k	turbulent kinetic energy
D	diameter of the jet	q_{pl}	constant surface heat flux on the plate
H	nozzle-to-plate distance	$\overline{v^2}$	velocity scale for turbulent transport
L	turbulent length scale	y^+	wall-distance in 'wall coordinates'.
Nu	Nusselt number $Nu = hD/\kappa$		
Pr	Prandtl number $Pr = \mu C_p/\kappa$		
Pr_t	turbulent Prandtl number		
Re_D	Reynolds number $Re_D = U_{jet}D/\nu$	Greek symbols	
T	turbulent time scale	Θ	temperature
U	mean velocity	Θ_{in}	inlet temperature
U_{jet}	jet bulk velocity	Θ_w	wall temperature
T^+	temperature in 'wall' coordinates	ε	dissipation rate of turbulence
f	variable related to energy redistribution	κ	thermal conductivity
		μ	fluid dynamic viscosity
h	wall heat transfer coefficient $h = q_{pl}/(\Theta_w - \Theta_{in})$	ν	fluid kinematic viscosity
		ν_t	turbulent kinematic viscosity.

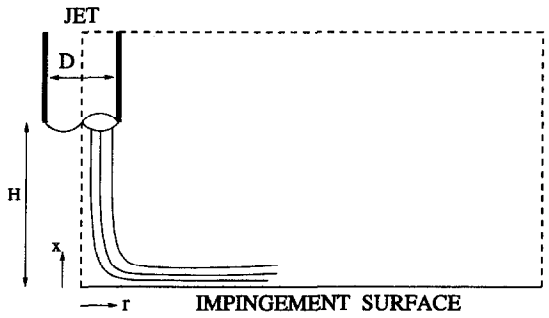

Fig. 1. The geometry and computational domain.

fer behavior of the jet for various jet to target distances and Reynolds numbers is analyzed.

2. AVAILABLE EXPERIMENTAL DATA

Cooper *et al.* [5] have recently reported a set of flow measurements at two different Reynolds numbers (i.e. $Re_D = 23\,000$ and $70\,000$); however, they did not make any heat transfer measurements. The purpose of their experiments was to provide hydrodynamic data for the heat transfer experiments of Baughn and Shimizu [6]. Baughn and Shimizu used a fully-developed jet striking a gold-coated, constant heat flux plate that was painted by liquid crystals for temperature measurements. They made measurements for several jet to plate-spacings ($H/D \geqslant 2$). In a later study by Baughn *et al.* [7], the same test rig was used to study the entrainment effects in a heated jet. They noted that their unheated jet results agreed with the earlier data of Baughn and Shimizu.

Lytle [13] also made heat transfer and flow measurements in an impinging air jet. He used an infrared thermal imaging system for temperature measurement and the velocity was measured by a Laser-Doppler Velocimetry (LDV) system. The focus of this study was on nozzle-to-plate spacings of less than one nozzle diameter. The results have been partly published in Lytle and Webb [9]. The relative size of the impingement plate (compared to the jet diameter) in this study was smaller than that of Baughn's experiments.

Yan [8] developed a transient measurement method using liquid crystals. He made local heat transfer coefficient measurements on the impingement test rig used in previous studies by Baughn *et al.* Yan notes that there was good agreement between his measurements and those of Baughn using the steady state method. Lee *et al.* [14] also used a test rig similar to Baughn *et al.* and made measurements at lower Reynolds numbers ($Re_D < 15\,000$).

3. NUMERICAL MODEL

3.1. *The V2F model*

The mean flow satisfies the Reynolds Average Navier–Stokes (RANS) equations, where the turbulent stresses are represented with an eddy-viscosity:

$$D_t U = -\nabla P + \nabla \cdot ((\nu + \nu_t)(\nabla U + \nabla' U)) \quad (1)$$

$$\nabla \cdot U = 0 \quad (2)$$

The V2F model used for evaluating ν_t is a general model, valid up to the wall and therefore, it does not require the use of any kind of wall functions (or other approximations), whose universality is more and more questionable, especially in impinging flow situations. The definition of the turbulent viscosity ν_t needs the evaluation of one time scale, T, and one velocity scale. For the latter, the variable $\overline{v^2}$ has been introduced by Durbin [15] instead of the turbulent kinetic energy k

used in the k–ε model, i.e. $\nu_t = C_\mu \overline{v^2} T$. $\overline{v^2}$ might loosely be regarded as the velocity fluctuation normal to the streamlines; note that it generally is not the y-component of velocity. Near to surfaces $\overline{v^2}$ behaves as the wall normal component of turbulent intensity. By arguing that the physical time scale cannot be smaller than the Kolmogorov time scale, Durbin [16, 17] derived the following expression, that prevents $1/T$ becoming infinite at the wall:

$$T' = \max\left(\frac{k}{\varepsilon}; 6\left(\frac{\nu}{\varepsilon}\right)^{1/2}\right) \tag{3}$$

Moreover, Durbin [18] recently considered a realizability constraint, in the context of impinging flows, and derived an upper bound for this time scale:

$$T = \min\left(T', \frac{\alpha}{2\sqrt{3}}\frac{\overline{v^2}}{k}\frac{k}{C_\mu\sqrt{S^2}}\right), \tag{4}$$

with $S^2 \equiv S_{ij}S_{ij}$, $S_{ij} = 1/2(\partial_i U_j + \partial_j U_i)$. Here, α is a model parameter which has to be positive and smaller than 1. Comparison of our computations with experimental data indicate that $\alpha = 0.6$ is a suitable value; larger values result higher heat transfer rates (this is discussed later in the results section), while smaller values would contradict the findings of previous computations for several flow types [12].

Transport equations are solved for the turbulent kinetic energy, k, its rate of dissipation, ε, and the transport velocity scale, $\overline{v^2}$:

$$\begin{aligned}
D_t k &= P - \varepsilon + \nabla\cdot\left(\left(\nu + \frac{\nu_t}{\sigma_k}\right)\nabla k\right)\\
D_t \varepsilon &= \frac{C'_{\varepsilon_1}P - C_{\varepsilon_2}\varepsilon}{T} + \nabla\cdot\left(\left(\nu + \frac{\nu_t}{\sigma_\varepsilon}\right)\nabla\varepsilon\right)\\
D_t \overline{v^2} &= kf - \frac{\overline{v^2}}{k}\varepsilon + \nabla\cdot\left(\left(\nu + \frac{\nu_t}{\sigma_k}\right)\nabla\overline{v^2}\right)
\end{aligned} \tag{5}$$

P is the turbulent kinetic energy production rate, $P = 2\nu_t S^2$. It should be noted that no damping functions are used in the model equations. The k and ε equations are similar to the k–ε model, except for the destruction term of ε where ε/k is replaced by $1/T$ to avoid a singularity at no-slip walls. C'_{ε_1} has been chosen as a function of the distance to the closest boundary d, in order to give suitable values of C'_{ε_1} for both turbulent boundary layer ($C'_{\varepsilon_1} = 1.55$) and plane mixing layer ($C'_{\varepsilon_1} = 1.3$): $C'_{\varepsilon_1} = 1.3 + 0.25/[1 + (d/2l)^2]^4$. l is a turbulent length scale, defined as $l = L/C_L$, with L given by equation (7). In parallel shear flow, the term kf represents the redistribution of turbulent intensity from the streamwise to the wall-normal component. Non-local effects of the impermeable solid boundaries are represented by the equation for f; this is a Helmholtz-type elliptic relaxation equation [16]:

$$f - L^2\nabla^2 f = (C_1 - 1)\frac{(2/3 - \overline{v^2}/k)}{T} + C_2\frac{P}{k} \tag{6}$$

Finally, by using the same approach as for the time scale, the following expression of the turbulent length scale is obtained.

$$\begin{aligned}
L' &= C_L \max\left(\frac{k^{3/2}}{\varepsilon}; C_\eta\left(\frac{\nu^3}{\varepsilon}\right)^{1/4}\right)\\
L &= \min\left(L', \frac{1}{\sqrt{3}}\overline{v^2}\frac{k^{3/2}}{C_\mu\sqrt{S^2}}\right)
\end{aligned} \tag{7}$$

The V2F model is valid up to the wall. No-slip boundary conditions are applied to the mean flow on solid boundaries; for the turbulence quantities, we impose $k = \partial_n k = 0$, $\overline{v^2} = 0$ and $\overline{v^2} = O(x_n^4)$. The constants of the model are [12]:

$$C_{\varepsilon_2} = 1.9, C_\mu = 0.19, C_1 = 1.4, C_2 = 0.3,$$

$$\sigma_k = 1.0, \sigma_\varepsilon = 1.3, C_L = 0.3, C_\eta = 70.0$$

3.2. *Turbulent Prandtl number*

In the mean temperature equation (the specific heat C_p is supposed to be constant), it is customary to represent turbulent transport of heat by defining a turbulent Prandtl number, which is the ratio of the momentum to heat eddy diffusivities:

$$D_t\Theta = \nabla\cdot\left(\left(\frac{\nu}{Pr} + \frac{\nu_t}{Pr_t}\right)\nabla\Theta\right) \tag{8}$$

There is substantial experimental data available on the turbulent Prandtl number (Pr_t). These are primarily based on measurements of T^+ in the log-region of a flat plate boundary layer. For air, with a molecular Prandtl number of $Pr = 0.71$, the data range between $Pr_t = 0.73$ and 0.92 [19]. The variation of the molecular Pr in the range of 0.7 to 64 (i.e. gases and most liquids including oils and with the exception of liquid metals) does not strongly affect the turbulent Prandtl number; according to Kays [19], a value of 0.85 is generally acceptable.

There are also a number of analytically determined relationships for turbulent Prandtl number in the literature. For instance, the DNS results of Kim and Moin [20] for fully developed flow of air in a duct indicate a $Pr_t \approx 1.2$ at the wall with a non-monotonic decrease to about 0.7 far from the wall. This behavior is in qualitative agreement with measurements in air, which according to Kays and Crawford [21] can be represented with a relationship of the form

$$Pr_t = \frac{1}{0.5882 + 0.228(\nu_t/\nu) - 0.0441(\nu_t/\nu)^2\left[1 - \exp\left(\frac{-5.165}{(\nu_n/\nu)}\right)\right]} \tag{9}$$

This formula yields a value of 1.7 at the wall with a

sharp decrease in its vicinity and an asymptotic value of 0.85 far from the wall. For the heated flat plate flow, computations of Durbin [15] adopting this formula and the widely used constant value of 0.9 have indicated a change of 10% in the Stanton number. In fact, these computations showed that the constant Pr_t value yields a marginally better agreement with experiments.

Measurements of Pr_t in other geometries are rather rare. Chua and Antonia [22] made measurements in a circular jet of air and showed a non-monotonic variation of Pr_t between 0.84 at the axis and 1.6 near the jet edge. They suggest a constant value of 0.81 in the region between the axis and the jet half-radius point. Several widely used Pr_t values were tested in the present computations: 0.73, 0.85, 0.92 and the Kays and Crawford formula. The results were not very sensitive to the Pr_t model.

4. SIMULATIONS AND COMPARISON WITH EXPERIMENTS AT A FIXED REYNOLDS NUMBER ($Re_D = 23\,000$)

4.1. *Computational approach*

Figure 1 is a sketch of the computational domain. All computations were performed with a general geometry, finite difference code developed by Rogers and Kwak [23]. The spatial discretization of convective terms was via a third order, upwind biased scheme; diffusion terms were central differenced. A fine, non-uniform, orthogonal, cylindrical grid of 120×120 cells was used, with a high resolution near all solid boundaries. A mesh sensitivity was performed by dividing the mesh by three in both directions. This changed the impingement region Nusselt number by less than 0.5% (Fig. 2). Therefore, the 120×120 grid was considered adequate. For high aspect ratios ($H/D \geqslant 10$) a 160×160 grid was used.

The flow conditions at the nozzle exit affect the computed flow field. Therefore, instead of specifying a boundary condition at the nozzle exit, we performed the computations in two steps. First, a fully-developed turbulent pipe flow was computed using 240 grid points in the radial direction. In this computation, the grid spacing was chosen such that at least five points were located in the region of $y^+ \leqslant 5$. This solution was then interpolated onto the full grid to provide the inlet condition of the jet. The flow domain began approximately two pipe diameters upstream of the jet exit, as shown in Fig. 1, so that the fully-developed turbulent pipe profiles may evolve in the nozzle as the flow approaches the jet exit. It is noted that prescribing the inlet conditions upstream of singularities is a well-known requirement also in other types of flows, e.g. the backward-facing step. Further, this allows the upper computational boundary to be sufficient distance from the wall that it does not affect the flow near the impingement surface. Finally, the effect of the jet wall thickness on the flow can be properly modeled. A constant static pressure condition was specified on the upper and right boundaries. We examined the effect of the right boundary location on the flow and thermal fields: we found that once this was larger than $(8 + H/D)$, there was no noticeable effect on the flow field and local Nusselt number. Two values of the pipe wall thickness were examined, 0.112D and 0.0313D, corresponding to the experiments of Baughn and Shimizu [6] and Cooper *et al.* [5], respectively. No noticeable difference was observed. The former value was used for the computations.

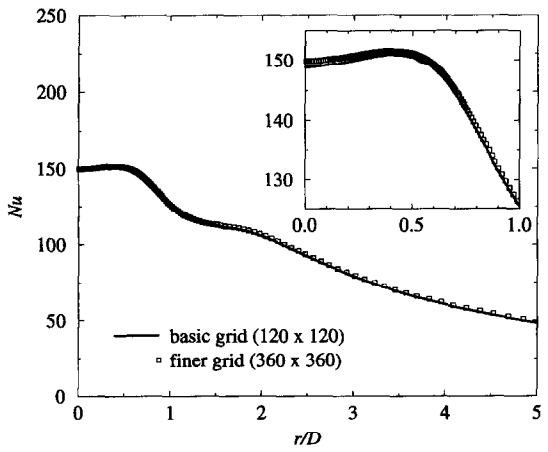

Fig. 2. Grid-independence of the solution; inset shows a magnified view of the stagnation region.

Simulations were first performed for a fixed jet Reynolds number of $Re_D = 23\,000$ and various aspect ratios, $0.5 \leqslant H/D \leqslant 14$ using both the k–ε and V2F models. Then we studied the influence of Reynolds number on the computational results. All computations have been conducted with a Prandtl number of 0.71. The V2F simulations required several hundred iterations for convergence, which took several minutes of CPU time on a Cray C90. In general, the k–ε simulations required double this number of iterations and a greater CPU time. For the k–ε model we used a damping function of the form $v_t = 0.09\, kT[1 - \exp(-0.01|kT/\nu|)]$, which yields similar behavior to the model of Launder and Sharma. Craft *et al.* [10] also used the Launder and Sharma model for the same problem and our k–ε predictions are similar to theirs.

4.2. *Preliminary computations*

The effect of the realizability constraint parameter α on the computational results was determined by using two different values, 0.6 and 1. For $H/D = 2$, the computed local Nusselt number is compared with the measured data in Fig. 3(a). Note that near the impingement region, a somewhat better agreement is obtained for $\alpha = 0.6$; however, downstream of this region and for $r/D \geqslant 2$, there is very little difference between the two predicted results. In this region, both values yield an excellent agreement with the data. The experimental data indicate a dip in the Nusselt number

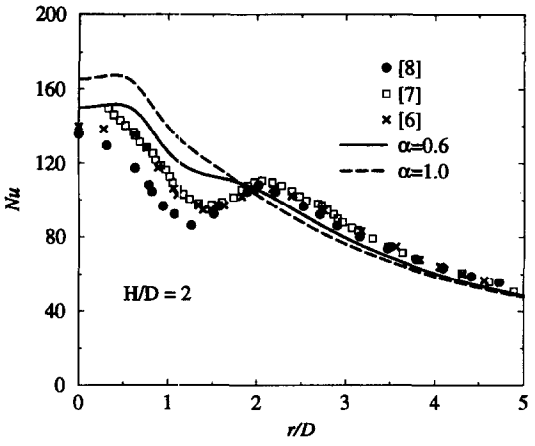

(a)

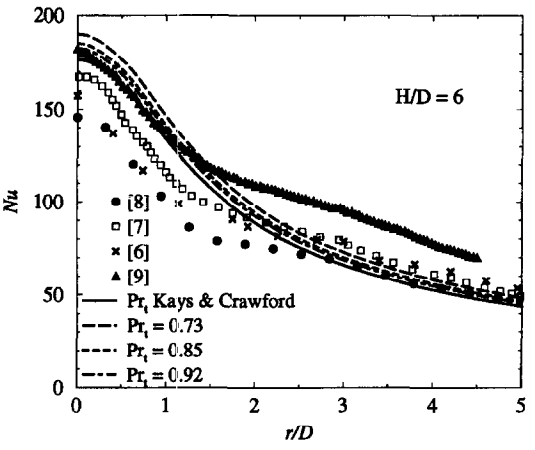

(b)

Fig. 3. Effect of (a) the realizability constant and (b) Pr_t on the local Nusselt number.

around $r/D = 1.4$, with a secondary peak occurring around $r/D = 2$. This behavior seems to be better represented by the simulation with $\alpha = 0.6$, which is the value we chose for all subsequent computations.

The effect of the turbulent Prandtl number, Pr_t, on the local Nusselt number for $H/D = 6$ is shown in Fig. 3(b). The results are not very sensitive to this parameter, especially downstream of the impingement region. Considering the scatter in the experimental data, it is difficult to say which value of Pr_t more closely fits the data. In the stagnation region, both $Pr_t = 0.92$ and the Kays and Crawford formula are in excellent agreement with the measurements of Lytle and Webb but are slightly higher than the data of Baughn *et al.* Away from this region, as the flow becomes parallel to the plate and forms the wall jet region, the prediction with $Pr_t = 0.73$ follows the data of Baughn and Shimizu, Baughn *et al.* and Yan. In this region, all predictions are below the measurements of Lytle and Webb. One possible explanation for the higher values of Nusselt number measured by Lytle and Webb is their use of a shorter length impingement plate. As the Kays and Crawford Pr_t formula yields a somewhat better agreement in the impingement region, subsequent simulations were performed with this formula.

4.3. *Results for* H/D = 2

The computed flow field for this case is shown by contours of the Stokes streamlines in Fig. 4 (for clarity, only part of the domain is shown). At the nozzle exit, these are parallel to the jet axis, representing the potential core of the jet. Near the stagnation region, the flow decelerates in the axial direction and turns, as exhibited by the sharp curvature in the streamlines. Past this region, and roughly for $r/D > 1.5$, a radial wall jet parallel to the plate begins to form with a developing boundary layer. Ambient fluid outside the free jet is entrained into the core with a developing shear layer separating the core and the ambient fluid. The entrainment is clearly evident by the curving of the streamlines outside the pipe towards the core of the jet. This leads to the formation of a recirculation region in the vicinity of the pipe-wall (a magnified view of this region is shown as an inset in Fig. 4). The features of the flow in this region are well captured by our computations indicating a sufficient grid resolution around the exit of the nozzle and in the shear layer.

For this aspect ratio, Cooper *et al.* [5] have made velocity measurements at various radial locations. A comparison of the measured velocity magnitude and our computations with the k–ε and V2F models at four different radial locations are shown in Fig. 5. On the stagnation streamline ($r/D = 0$) there is very little difference between the two predictions and quite a good agreement with the experimental data is noted. At $r/D = 0.5$, the k–ε model predicts lower velocities than the V2F which yields a slightly better agreement near the wall. In the wall jet region, at $r/D = 1$, the V2F model correctly predicts the flow acceleration; there is excellent agreement with the data near the wall, with a slight over-prediction in the outer region. At this radial location, the k–ε model predicts low velocities in the wall region and high velocities in the outer region. Further downstream, the flow decelerates and again the V2F model correctly predicts this behavior, showing very good agreement with the experiment at $r/D = 2.5$. The k–ε model does not cor-

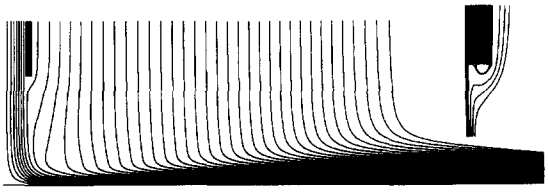

Fig. 4. Streamlines for $H/D = 2$ computed with the V2F model; inset shows a magnified view of the flow near the pipe exit.

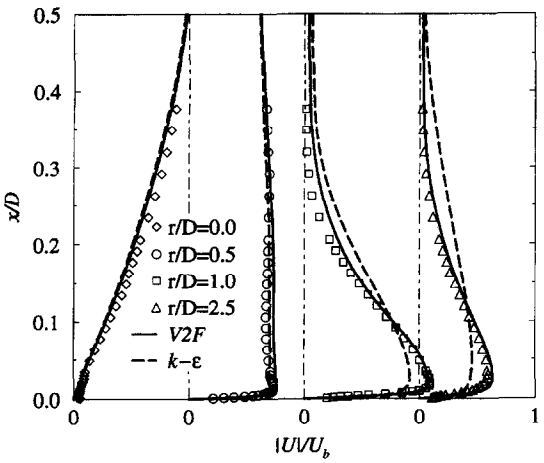

Fig. 5. Profiles of the velocity magnitude normalized by the bulk velocity of the jet at various radial locations, symbols: [5].

rectly resolve the development of the boundary layer, leading to an under-prediction of the velocity in the wall region and an over-prediction in the outer region. The origin of the discrepancy between the k–ε predictions and data will be discussed later.

In the stagnation region, the k–ε model significantly over-predicts the local Nusselt number, as seen in Fig. 6. In this model, the stagnation Nusselt number is about 170% higher than the measured value, whereas the V2F model prediction is only about 9% too high. Downstream of the stagnation region, the k–ε Nusselt number rapidly decreases and approaches the experimental and V2F values.

The experimental data indicate a dip in the local Nusselt number distribution around $r/D = 1.4$ and a secondary maximum at around $r/D = 2$. The data of Yan [8] indicate a more pronounced local minimum

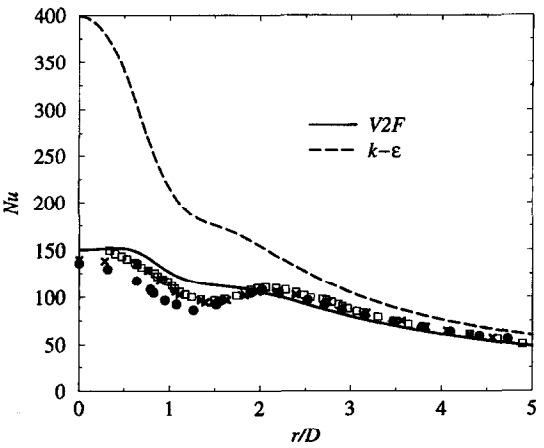

Fig. 6. Distribution of local wall heat transfer coefficient for $H/D = 2$; for experimental data symbol key, see Fig. 3.

of Nusselt number than those of refs. [7, 6]. Also, in the data of Yan this point is shifted closer to the stagnation point with a somewhat lower value of Nu in the region $r/D < 1.5$. The V2F model does not predict a local secondary maximum, however it does show a deflection in the local Nusselt number distribution. It can be said that the agreement between the data and the V2F computation is quite good in the regions $r/D \leqslant 1$ and $r/D \geqslant 1.8$.

Some investigators [14] have attributed the local maximum to transition from a laminar to turbulent boundary layer in the wall jet region. This is not supported by the measurements of Lytle and Webb [9] who note that there are relatively high levels of turbulence even in the stagnation region. It is believed that an increase in the turbulent kinetic energy away from the stagnation region is responsible for this local increase of Nu. This was observed by Lytle and Webb and is predicted by the present model, as illustrated by Fig. 7. The increase in the turbulent energy is produced by high shear in the region of streamline convergence, away from the stagnation point, where the turbulent shear layer is impinging on the plate. This is supported by the experimental observations of Popiel and Trass [24], who showed that there exists a strong axisymmetric toroidal vortex in this region.

The anomalously high Nusselt number predicted by k–ε can be attributed to erroneous physics. The impinging potential core of the free jet contains low levels of turbulence and these should remain relatively low in the stagnation region. The V2F predictions are consistent with this expectation. However, the k–ε model generates a spurious kinetic energy maximum near the stagnation point, as illustrated by Fig. 7. This figure is a composite: on the left half are contours of k predicted by k–ε and on the right predictions of V2F. The contours on the left show a pronounced maximum near the surface, on the jet axis. This is responsible for the excessive level of the stagnation point Nusselt number.

The maximum value of k predicted by the k–ε model is 80% higher than that of V2F. The location of this maximum, shown by the arrows on Fig. 7, is in the stagnation region for the k–ε, and at about $r/D = 2$ for the V2F. The behavior predicted by the V2F model is qualitatively confirmed by measurements of Lytle and Webb [9], in the sense that they also noted an increase of the turbulent intensity away from the stagnation region, with an off-axis maximum.

Single, hot-wire measurements of velocity fluctuations normal to the plate are shown in Fig. 9. For comparison, we have also plotted $2/3\,k$ from both k–ε and V2F computations as well as $\overline{v^2}$ from the V2F computation. This figure clearly shows that in the near-wall region, and in particular around the stagnation point, $\overline{v^2}$ is behaving like the normal component of velocity. k predictions from the k–ε model are one order of magnitude higher than $\overline{v^2}$; hence this model drastically over-estimates the turbulent momentum and heat transfer rates.

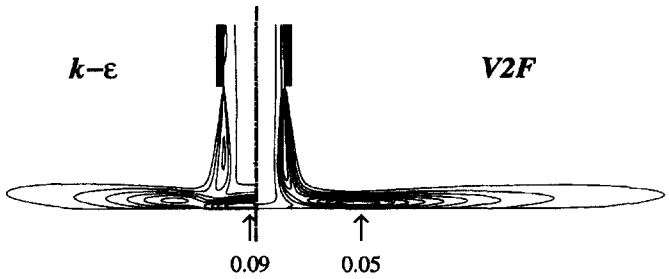

Fig. 7. Contours of turbulent kinetic energy for $H/D = 2$.

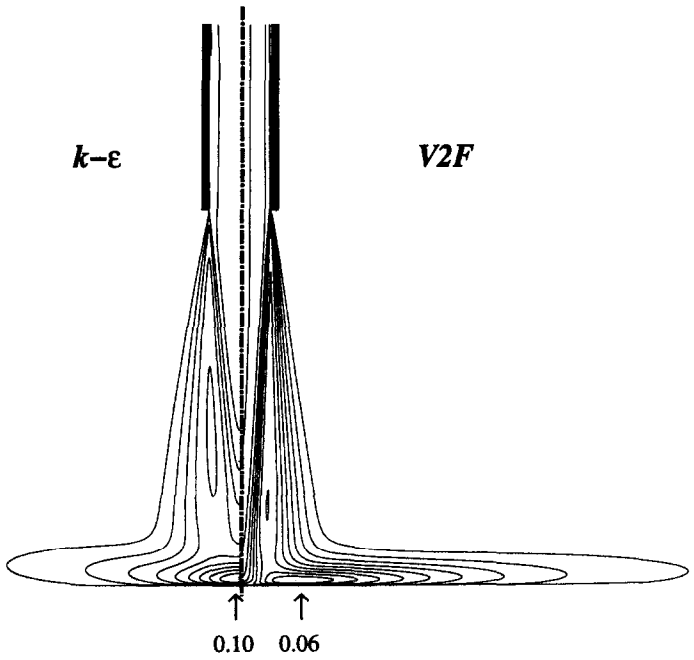

Fig. 8. Contours of turbulent kinetic energy for $H/D = 6$.

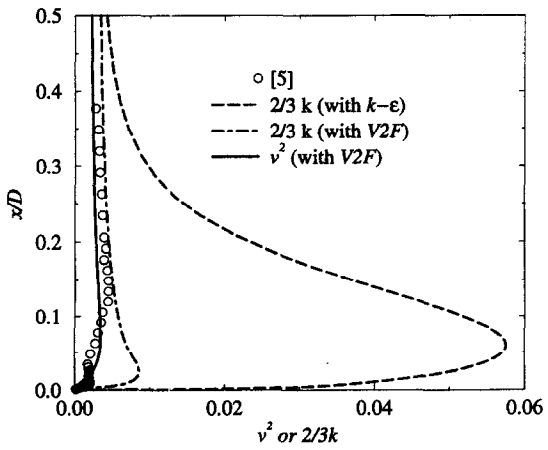

Fig. 9. Velocity fluctuations (squared) on the stagnation line ($H/D = 6$).

4.4. *Results for* H/D = 6

The contours of the turbulent kinetic energy for the case of $H/D = 6$ are shown in Fig. 8. The maximum value of k predicted by the k–ε model is 66% higher than V2F. The location of this maximum, shown by the arrows on this figure, is in the stagnation region for the k–ε, and at about $r/D = 1$ for the V2F. Again the prediction by the k–ε model is anomalous in magnitude and location.

A comparison of the predicted and measured local Nusselt numbers is presented in Fig. 10. In the impingement region, there is a 25% scatter in the experimentally measured Nusselt number. The data of Lytle and Webb [9] are consistently higher than other measurements. The k–ε model over-predicts the stagnation Nusselt number by about 120% but the discrepancy gradually reduces moving away from the

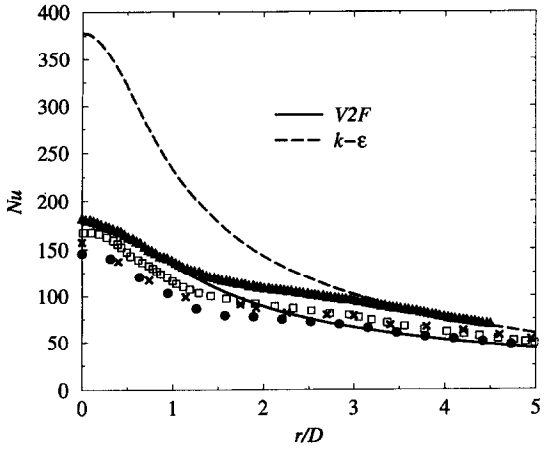

Fig. 10. Distribution of local wall heat transfer coefficient for $H/D = 6$; for experimental data symbol key, see Fig. 3.

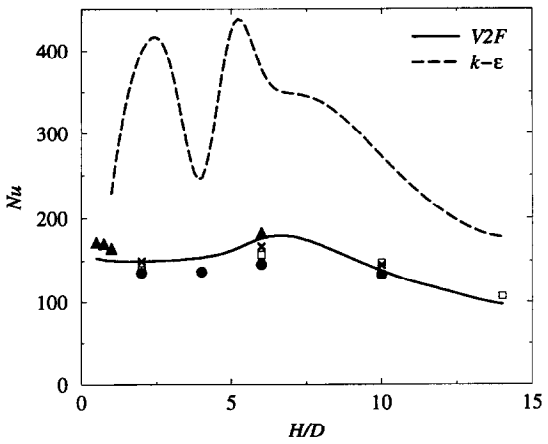

Fig. 11. Effect of jet distance on the heat transfer at the stagnation point; for experimental data symbol key, see Fig. 3.

impingement region. The V2F model prediction is in excellent agreement with the data of Lytle and Webb in the impingement region; however in the wall jet region, it is in better agreement with the data of Yan [8]. Unlike the lower aspect ratio results ($H/D = 2$), there is no secondary maximum in the Nusselt number distribution. This is believed to be due to the fact that as the jet is moved further out from the impingement surface, the location of maximum k moves closer to the jet axis. This is supported by the computations with the V2F model which predicts the location of this point to lie at $r/D \simeq 2$ and $r/D \simeq 1$ for aspect ratios of two and six, respectively.

4.5. *Stagnation Nusselt number*

Simulations have been carried out for a constant Reynolds number ($Re_D = 23\,000$) and a wide range of aspect ratios ($0.5 \leqslant H/D \leqslant 14$) to determine the dependence of the stagnation Nusselt number on H/D. This dependence is crucial to many applications of impingement cooling. A comparison of the computed values with the experimental data is presented in Fig. 11. The V2F model predictions are in good agreement with the data. Experimental measurements [6, 8, 14] have indicated that for $H/D > 1$, the stagnation Nusselt number exhibits a maximum value at around $H/D = 6$. Our computations confirm this finding and indicate that the maximum stagnation Nusselt number is between H/D of six and seven. This might be attributed to the increase in the turbulent kinetic energy as the jet is moved away from the impingement surface. For instance, as previously discussed, the maximum of k at $H/D = 6$ is higher than that of $H/D = 2$. This explanation is supported by Kataoka *et al.* [25] who show that turbulent intensity reaches a maximum at an aspect ratio of seven. The measurements of ref. [9] also indicate that at lower spacing ratios, the stagnation Nusselt number goes through a local minimum at $H/D = 1$ which is also correctly predicted by the V2F model.

The k–ε model substantially over-predicts the stagnation Nusselt number. Fig. 11 also indicates a behavior unlike the trend observed in the experiments and the V2F computations. Two pronounced maxima are predicted around H/D of three and five with a local minimum around four. At higher aspect ratios, the k–ε predictions gradually approach the measurements.

5. BEHAVIOR WITH INCREASING REYNOLDS NUMBER

All the previous computations have been conducted at a Reynolds number of 23 000. Although the V2F results are excellent in comparison to state of the art turbulence models, it is essential to check its accuracy at different Re_D. Turbulence models are sometimes fitted for a given test-case, at a given Reynolds number and might give much worse results when flow conditions are changed. In this study, we used stagnation point data solely in the selection of the realizability constant, α. All other constants had been found previously from simple, parallel shear flow data.

Higher Reynolds number data are provided by the recent experiments of Cooper *et al.* [5] for the fluid flow and Yan [8] for the heat transfer. These data are at $Re_D = 50\,000$ and 70 000. In this section, we will focus only on the latter data, in order to provide the largest span of Reynolds number.

First, some velocity magnitude profiles have been made available at $Re_D = 70\,000$ in ref. [5]. Figure 12 shows the comparison of the V2F model with these experimental data. Again, as for $Re_D = 23\,000$, one can see a very good agreement at several radial locations. The V2F model accurately predicts the initial flow acceleration, then deceleration in the developing boundary layer. So the predicted flow pat-

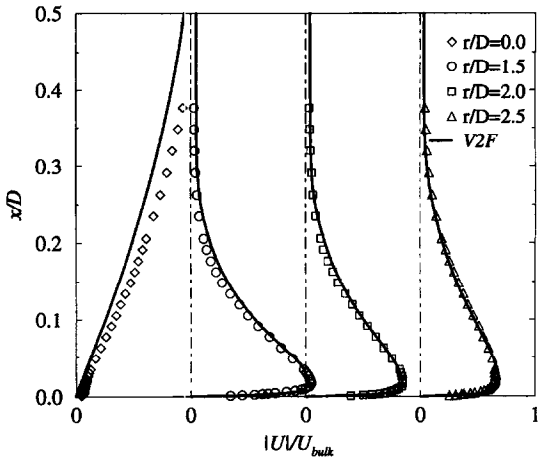

Fig. 12. Profiles of the velocity magnitude normalized by the bulk velocity of the jet at various radial locations, at $Re_D = 70\,000$ for $H/D = 2$, symbols: [5].

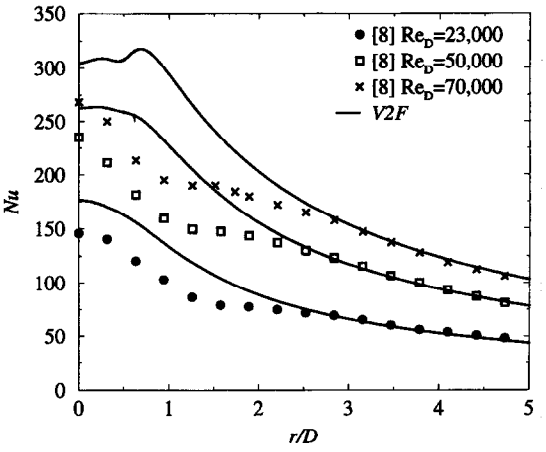

Fig. 14. Distribution of local wall heat transfer coefficient for $H/D = 6$ at different Reynolds numbers.

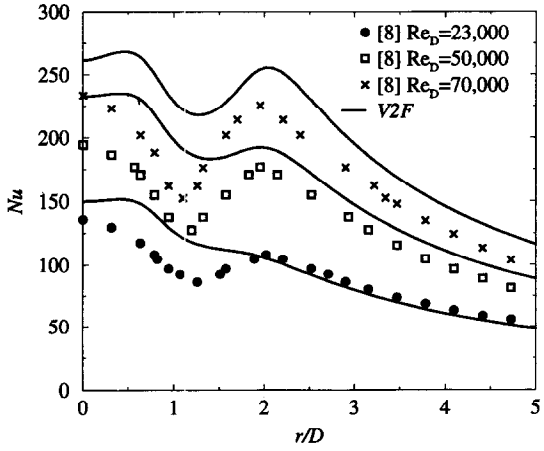

Fig. 13. Distribution of local wall heat transfer coefficient for $H/D = 2$ at different Reynolds numbers.

tern shows the right qualitative and quantitative behavior of when Re_D is varied.

The evolution of the local Nusselt number on the flat plate while increasing Reynolds number is presented for two nozzle-to-plate distances in Figs. 13 and 14. Comparisons are with Yan's [8] experimental data. For $H/D = 2$, one observes in Fig. 13 an augmentation with Re_D of the relative height of the secondary peak in the Nu distribution. The model is qualitatively consistent with the experiment. As for the lower Reynolds number, this peak is less pronounced in the computations, but its location is very well predicted (around $r/D = 2$). Recall that a 20% scatter existed in the experimental data at $Re_D = 23\,000$ and that Yan's data were systematically close to the lowest quantitative bound on the whole set of available data. In light of this, the V2F results may be considered quite good.

For $H/D = 6$ (Fig. 14), the agreement is still reasonable, especially in comparison to dramatic k–ε predictions, which have on the order of a 100% error in the stagnation region. However, a spurious peak, which does not seem to exist in the experiment, appears around $r/D = 0.8$ in the computations at $Re_D = 70\,000$. We do not know yet the origin of this peak.

Finally, we evaluated a data correlation of the form $Nu_{stag} = a(Re_D)^{\beta}$. Fig. 15(a) and (b) show log–log plots, from which β has been determined. The V2F simulations follow very similar trends to the experiment with only slightly over-predicted values of stagnation Nusselt number, as it has been noted previously. For $H/D = 2$, β has been evaluated as 0.51, against 0.47 in the experiment; for $H/D = 6$, V2F gives the value of 0.49 against 0.56 in Yan's data. These exponents have been evaluated only with 3 points, so they are subject to uncertainty, but the 1/2 slope in the stagnation region, widely cited in the literature [8, 9, 14], is well predicted by the V2F model. Of course, the Nu data do not follow $Re_D^{1/2}$ at locations away from the stagnation point. It might be reasonable to regard the stagnation region as 'quasi-laminar', in the sense that k is relatively low there, but there is not a laminar to turbulent transition with increasing radius. It is simply a matter of moving from the potential core to wall jet region of the impingement flow.

6. CONCLUSION AND FUTURE PLANS

The main aim of this research has been to assess the ability of computational fluid mechanics and heat transfer to accurately and economically predict the heat transfer rate in an impinging jet. The computations carried out herein show that predictions by the normal-velocity relaxation model (V2F model) agree very well with the experiments. The k–ε model does not properly represent the flow features, highly over-predicts the rate of heat transfer and yields physi-

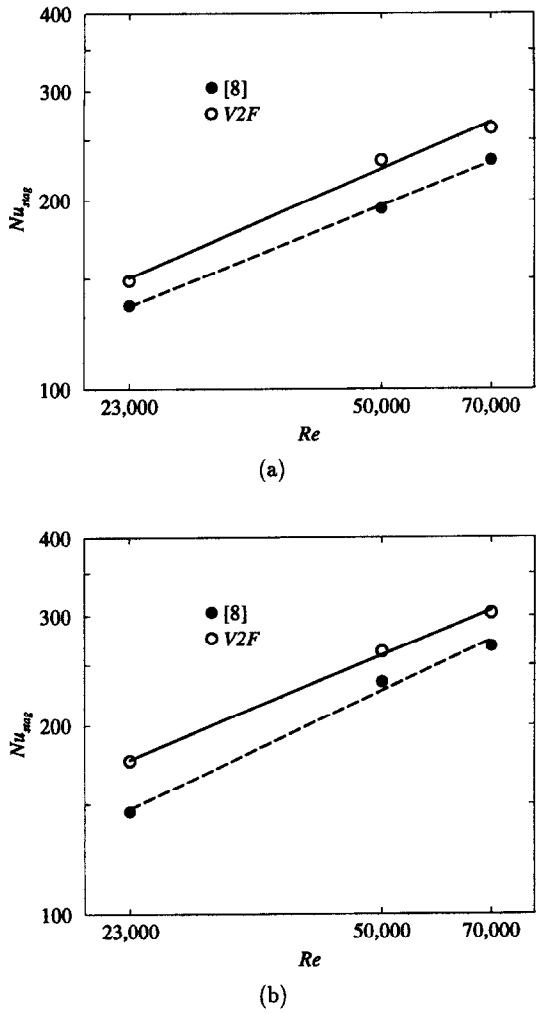

Fig. 15. Effect of Reynolds number on the stagnation Nusselt number; (a) $H/D = 2$ and (b) $H/D = 6$.

cally unrealistic behavior. Computations not reported here show that using the 'RNG' coefficients for the k–ε model produces results quite similar to those presented here for the standard, constant coefficient version. In particular, the excessive production of k in the stagnant point region is not alleviated by the altered set of coefficients. Computations were also done with wall functions instead of damping functions, and with a commercial CFD code. In all cases, the k–ε model excessively over-predicted the stagnant point value of Nu.

It is planned to perform additional two and three dimensional computations to cover a wider range of parameters, such as the geometry and molecular Prandtl number. In particular, for electronic cooling applications, dielectric liquids in a confined jet geometry need to be explored. There are also some recent experimental measurements of heat transfer from a pedestal being cooled by an impinging jet which will be used for comparison with future simulations. The understanding gained and the results obtained can be directly relevant to a number of industrial and engineering applications.

Acknowledgements—We thank Profs Baughn (University of California, Davis), Webb (Brigham Young University) and Yan (Southern Illinois) for providing their experimental data. Cooper *et al.*'s data have been obtained from the ERCOFTAC database (http://fluindigo.mech.surrey.ac.uk).

REFERENCES

1. Martin, H., Heat and mass transfer between impinging gas jets and solid surfaces. *Advances in Heat Transfer*, 1977, **13**, 1–60.
2. Downs, S. J. and James, E. H., Jet impingement heat transfer—a literature survey. ASME Paper No. 87-HT-35, 1987.
3. Viskanta, R., Heat transfer to impinging isothermal gas and flame jets. *Experimental Thermal and Fluid Science*, 1993, **6**, 111–134.
4. Nakayama, W., Heat transfer engineering in systems integration: outlook for closer coupling of thermal and electrical designs of computers. *IEEE Transactions on Components, Packaging, and Manufacturing Technology—Part A*, 1995, **18**(8), 818–826.
5. Cooper, D., Jackson, D., Launder, B. and Liao, G., Impinging jet studies for turbulence model assessment—I. Flow-field experiments. *International Journal of Heat and Mass Transfer*, 1993, **36**(10), 2675–2684.
6. Baughn, J. and Shimizu, S., Heat transfer measurements from a surface with uniform heat flux and an impinging jet. *Journal of Heat Transfer*, 1989, **111**, 1096–1098.
7. Baughn, J., Hechanova, A. and Yan, X., An experimental study of entrainment effects on the heat transfer from a flat surface to a heated circular impinging jet. *Journal of Heat Transfer*, 1991, **113**, 1023–1025.
8. Yan, X., A preheated-wall transient method using liquid crystals for the measurement of heat transfer on external surfaces and in ducts. Ph.D. thesis, University of California, Davis, 1993.
9. Lytle, D. and Webb, B., Air jet impingement heat transfer at low nozzle-plate spacings. *International Journal of Heat and Mass Transfer*, 1994, **37**, 1687–1697.
10. Craft, T., Graham, L. and Launder, B., Impinging jet studies for turbulence model assessment—II. An examination of the performance of four turbulence models. *International Journal of Heat and Mass Transfer*, 1993, **36**(10), 2685–2697.
11. Kunugi, T., Yokomine, T. and Ichimiya, K., Numerical and experimental study on heat transfer of an impinging turbulent plane jet with confined wall. *ASME HTD*, 1993, **246**, 25–31.
12. Durbin, P., Separated flow computations with the k–ε–v^2 model. *AIAA Journal*, 1995, **33**(4), 659–664.
13. Lytle, D., Air jet impingement heat transfer at low nozzle-to-plate spacings. M.S. thesis, Brigham Young University, 1990.
14. Lee, D., Greif, R., Lee, S. and Lee, J., Heat transfer from a flat plate to a fully developed axisymmetric impinging jet. *Journal of Heat Transfer*, 1995, **117**, 772–776.
15. Durbin, P., Application of a near-wall turbulence model to boundary layers and heat transfer. *International Journal of Heat and Fluid Flow*, 1993, **14**(4), 316–323.
16. Durbin, P., Near-wall turbulence closure without damping functions. *Theoretical and Computational Fluid Dynamics*, 1991, **3**(1), 1–13.

17. Durbin, P., A Reynolds-stress model for near-wall turbulence. *Journal of Fluid Mechanics*, 1993, **249**, 465–498.
18. Durbin, P., On the k–ε stagnation point anomaly. *International Journal of Heat and Fluid Flow*, 1996, **17**, 89–90.
19. Kays, W. M., Turbulent Prandtl number—where are we? *Journal of Heat Transfer*, 1994, **116**, 284–295.
20. Kim, J. and Moin, P., Transport of passive scalars in a turbulent channel flow. *Proceedings of 6th International Symposium on Turbulent Shear Flows*, 1987, pp. 5.2.1–5.2.6.
21. Kays, W. M. and Crawford, M. E., *Convective Heat and Mass Transfer*, 3rd Edn, McGraw-Hill, 1993.
22. Chua, L. P. and Antonia, R. A., Turbulent Prandtl number in a circular jet. *Journal of Heat Transfer*, 1990, **33**(2), 331–339.
23. Rogers, S. E. and Kwak, D., Upwind differencing scheme for the time-accurate incompressible Navier-Stokes equations. *AIAA Journal*, 1990, **28**, 253–262.
24. Popiel, C. and Trass, O., Visualization of a free and impinging round jet. *Experimental Thermal and Fluid Science*, 1991, **4**, 253–264.
25. Kataoka, K., Suguro, M., Degawa, K., Maruo, K. and Mihata, I., The effect of surface renewal due to large-scale eddies on jet impingement heat transfer. *International Journal of Heat and Mass Transfer*, 1987, **30**, 559–567.